



Detail investigation of thermoelectric performance and magnetic properties of Cs-doped $\text{Bi}_2\text{Sr}_2\text{Co}_2\text{O}_y$ ceramic materials

B. Özçelik¹ · M. Gürsul¹ · G. Çetin¹ · C. Özçelik² · M. A. Torres³ · M. A. Madre³ · A. Sotelo³

Received: 8 September 2020 / Accepted: 22 December 2020 / Published online: 12 January 2021

© The Author(s) 2021

Abstract

$\text{Bi}_2\text{Sr}_{2-x}\text{Cs}_x\text{Co}_2\text{O}_y$ materials with $0 \leq x \leq 0.15$, have been fabricated via the classical ceramic technique. XRD results have indicated that undoped and Cs-substituted samples are composed of $\text{Bi}_2\text{Sr}_2\text{Co}_2\text{O}_y$ phase as the major one. Microstructural studies have demonstrated the formation of a liquid phase, which allows a drastic grain growth. This factor is responsible for a drastic improvement of relative density, reaching about 95% of the theoretical one for 0.125 Cs content. On the other hand, electrical resistivity has been reduced up to 14 mΩ cm at 650 °C for 0.125 Cs content, around 40% lower than the obtained in undoped samples. As a consequence, Seebeck coefficient has been decreased due to the raise in charge carrier concentration. The highest power factor at 650 °C (0.21 mW/K² m) has been found for 0.125 Cs substituted sample, about 40% larger than the obtained in undoped samples, and very similar to the notified in single crystals (0.26 mW/K² m). Magnetisation with respect to temperature results have demonstrated that measured samples have a paramagnetic property above 50 K, except 0.10 Cs. Magnetic hysteresis curves have shown that the slopes and the magnitudes have increased with decreasing temperature.

Keywords $\text{Bi}_2\text{Sr}_2\text{Co}_2\text{O}_y$ · Electrical properties · Seebeck coefficient · Power factor · Layered cobaltites

1 Introduction

Since the establishment of fundamental equations to explain thermoelectric (TE) phenomena [1, 2], many different families of TE materials have been discovered [3–5]. Nowadays, the most attracting characteristic of these materials is their ability to directly transform, without the need of moving parts, heat into electric power [6]. The material efficiency to perform this process can be evaluated through the dimensionless ZT (Figure of Merit) obtained from [7]: ($ZT = S^2\sigma T/\kappa$), where S , σ , T , and κ , are Seebeck coefficient, electrical conductivity, absolute temperature, and thermal conductivity, respectively. Moreover, the $S^2\sigma$ factor, representing the electrical part in this expression is known as the TE Power Factor, PF.

Usually, it is considered that TE materials for practical applications should present $ZT \geq 1$. Recently, the largest ZT values have been obtained in intermetallic materials, as PbTeSe [3]. On the other hand, these materials show limited working temperatures due to oxidation at high temperature under air, very expensive costs [6], and less plenty in the earth crust [8]. However, in spite of the major abundance of silicon in the earth crust [8], the best performances are obtained in high costs materials [6]. The discovery of high TE properties in oxide materials [5], which combine high working temperatures, low costs and relatively high abundance in the earth crust [6, 8], opened a broad research field. Following this discovery, and provided by the important advantages of oxides, new materials with attractive TE properties, such as $\text{Bi}_2\text{Sr}_2\text{Co}_{1.8}\text{O}_x$ [9],

✉ B. Özçelik, ozcelik@cu.edu.tr | ¹Department of Physics, Faculty of Sciences and Letters, Çukurova University, 01330 Adana, Turkey. ²Institute of Engineering and Sciences, Iskenderun Technical University, Hatay, Turkey. ³Dpto. de Ciencia de Materiales, ICMA (CSIC-Universidad de Zaragoza), C/María de Luna 3, 50018 Saragossa, Spain.



were also found. Moreover, the interest in these materials grew when ZT of 1.2 in $\text{Bi}_2\text{Sr}_2\text{Co}_{1.8}\text{O}_x$ whiskers was achieved [10]. However, in spite of the many works published on TE oxides, bulk polycrystalline materials cannot reach these ZT values, being usually much lower than 1. As a consequence, one of the main objectives of researchers is enhancing their TE performances to be used in practical applications. Among the large number of approaches performed to enhance the TE properties of these oxides, it can be highlighted the use of wet-synthesis methods [11, 12], texturing [13, 14], and doping [15, 16].

The studies performed on TE oxides of the CoO family have allowed to determine that the substitution of any cation of the Rock Salt layer by a lower oxidation one, leads to an increase of charge carrier concentration due to the partial promotion of Co^{3+} cations to Co^{4+} in the conducting layer [17], which induces a decrease of Seebeck coefficient [18]. This effect can be produced by alkaline earth substitution in the structure by an alkaline element, leading to important microstructural and electrical modifications, as demonstrated in previous works [19, 20]. Therefore, we aim to determine the effect of a large alkaline cation (Cs) partial substitution in the alkaline earth position of $\text{Bi}_2\text{Sr}_2\text{Co}_2\text{O}_y$ thermoelectric compound. The structural and microstructural changes induced by this substitution will be determined and linked to the modifications of electrical properties in classically sintered materials.

2 Experimental

Cs-doped $\text{Bi}_2\text{Sr}_{2-x}\text{Cs}_x\text{Co}_2\text{O}_y$ precursors, with $0 \leq x \leq 0.15$, have been prepared, through the classical ceramic method, using commercial Bi_2O_3 (98+%, Panreac), SrCO_3 (98.5%, Panreac), CoO (99.99%, Sigma-Aldrich), and Cs_2CO_3 (99.8%, Panreac) powders as starting materials. After weighing them in the appropriate proportions, they were well mixed and subjected to ball milling, using water media, at 300 rpm for 30 min. The produced slip was subsequently dried and heated to decompose the carbonates using a two-step process: 750 °C for 12 h, and 800 °C for 12 h, with an intermediate manual milling. Finally, the powders were uniaxially pressed into pellets ($2 \times 2 \times 14 \text{ mm}^3$) under 400 MPa applied pressure, and sintered at 810 °C for 24 h and furnace cooled.

Powder X-ray diffraction (XRD) patterns were obtained in a Rigaku D/max-B X-ray powder diffractometer working with Cu K α radiation, and fixing 2θ between 10 and 40 degrees, in order to identify the phases in the textured materials. Microstructural characterization has been made in a Zeiss–Merlin field emission scanning electron microscope (FESEM) associated to an energy-dispersive spectroscopy (EDS) system used for qualitative elemental

analysis. Samples were analysed through surface micrographs to determine microstructural modifications induced by Cs doping. Moreover, density of materials has been obtained by Archimedes' method in several specimens for each composition to minimize errors.

Electrical properties of the different samples were determined through simultaneous measurement of Seebeck coefficient and electrical resistivity using the well-known direct current four-probe configuration in a LSR-3 system (Linseis GmbH). These properties have been obtained under steady-state conditions between 50 and 650 °C using He atmosphere. Electrical performance of samples, PF, was calculated using these data. Finally, the magnetic properties were measured by using a PPMS system (Dynecool PPMS, Quantum Design). The magnetic hysteresis data were taken in between—5 to 5 T, and the magnetization measurements were obtained in ZFC mode under a DC-field of 20 Oe, from 300 K down to 5 K.

3 Results and discussion

Representative XRD patterns obtained on grinded $\text{Bi}_2\text{Sr}_{2-x}\text{Cs}_x\text{Co}_2\text{O}_y$ materials are presented in Fig. 1. In this graph, it may be easily deduced that most of the peaks (indicated by their diffraction planes) can be associated to the $\text{Bi}_2\text{Sr}_2\text{Co}_2\text{O}_y$ phase, being the major one, which is

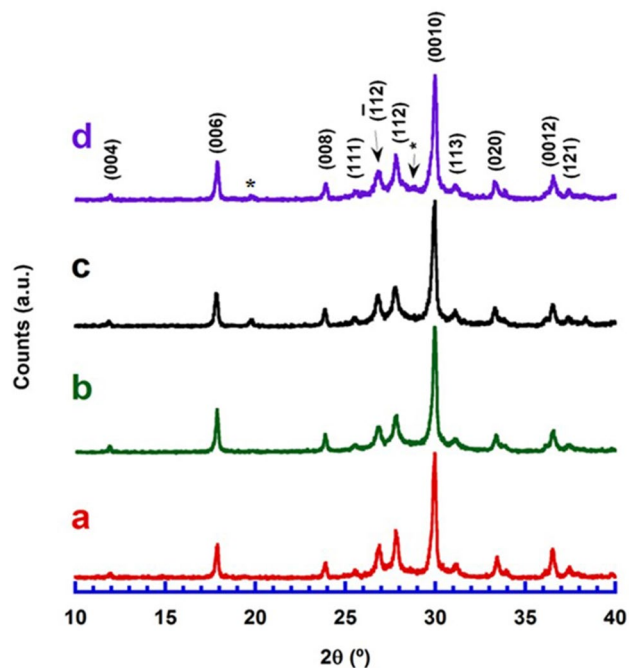


Fig. 1 Representative powder X-ray diffraction patterns of $\text{Bi}_2\text{Sr}_{2-x}\text{Cs}_x\text{Co}_2\text{O}_y$ samples; for $x =$ (a) 0; (b) 0.025; (c) 0.075; and (d) 0.125. Diffraction planes show the peaks associated to the TE phase, while * identifies the corresponding to the Bi–Sr–O phase

consistent with literature [21]. Moreover, the * shows the Co-free secondary phase [22], which is present in very small proportions. Consequently, it can be easily deduced that all samples are formed by nearly single $\text{Bi}_2\text{Sr}_2\text{Co}_2\text{O}_y$ phase. On the other hand, in comparison to undoped samples, very small shift in the diffraction peaks of Cs-doped samples has been found, resulting from higher ionic radius of Cs. In addition, no Cs-based secondary phases have been observed.

Figure 2 displays representative SEM micrographs performed on the surface of $\text{Bi}_2\text{Sr}_{2-x}\text{Cs}_x\text{Co}_2\text{O}_y$ samples. From these micrographs, it is easy to observe a drastic grain growth and decrease of porosity when the amount of Cs is increased. This evolution can be associated to the formation of a liquid phase induced by the alkaline cation, which can be due to the low melting point of Cs_2CO_3 (793 °C [23]), in agreement with previous studies on similar compounds [24]. Up to 0.05 Cs substitution (Fig. 2b), the grain sizes are only slightly larger than in pure samples (Fig. 2a). On the other hand, higher Cs additions lead to much larger grains, indicating the presence of a large amount of liquid phase along the grain boundaries, which enhances cations mobility. This effect, and the system tendency to decrease surface energy, are the responsible parameters for increasing grain sizes. On the other hand, another

important microstructural modification is the appearance, besides the grey contrast (#1, associated through EDS to the thermoelectric $\text{Bi}_2\text{Sr}_2\text{Co}_2\text{O}_y$ phase), of a light grey one (#2, corresponding to the Bi–Sr–O phase) when Cs is added to the samples. Finally, for the highest Cs containing samples, a black contrast can be found (#3), with Co-oxide composition. On the other hand, Cs doping leads to a slight Ca^{2+} by Cs^+ substitution, found by EDS analysis of the thermoelectric phase in several samples for each Cs substitution. The EDS results have shown that the substituting Cs amount corresponds to, approximately, one half of the nominal one in the inner part of the samples, while it is hardly detected in the surface of samples. Moreover, no Cs has been identified in any of the secondary phases. These data clearly agree with previous observations in similar compounds [24].

In order to determine the effect of this liquid phase in the sintering process, density measurements have been performed using Archimedes' method and the results are presented, as a function of nominal Cs content, in Fig. 3. As it can be observed in the graph, undoped samples display the lowest densities, 5.45 g/cm³, which are about 80% of the theoretical one (taking theoretical density as 6.8 g/cm³ [25]). When Cs is added, relative density monotonically increases with Cs content up to around 95% for 0.125 Cs

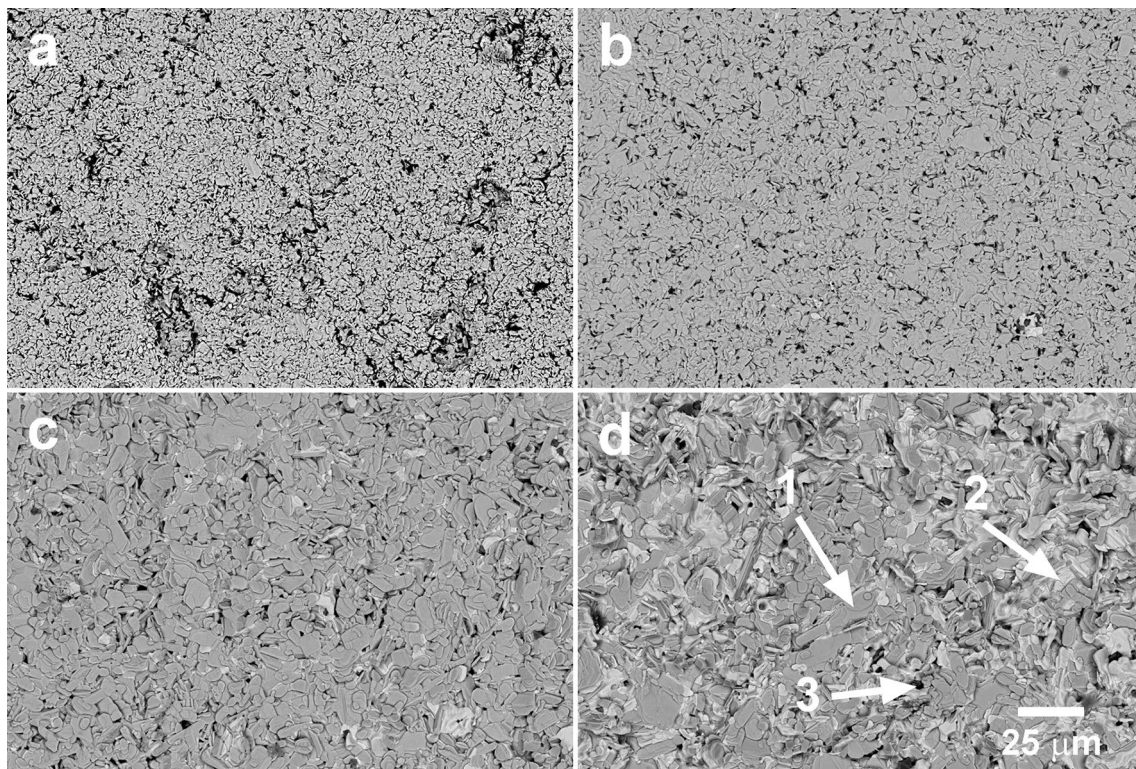


Fig. 2 Representative SEM micrographs performed on surfaces of $\text{Bi}_2\text{Sr}_{2-x}\text{Cs}_x\text{Co}_2\text{O}_y$ samples, with $x = \mathbf{a}$ 0; \mathbf{b} 0.05; \mathbf{c} 0.1; and \mathbf{d} 0.15. Grey contrast (#1) corresponds to the thermoelectric phase, light grey (#2) to the Co-free one (Bi–Sr–O), and black one (#3) to Co-oxide

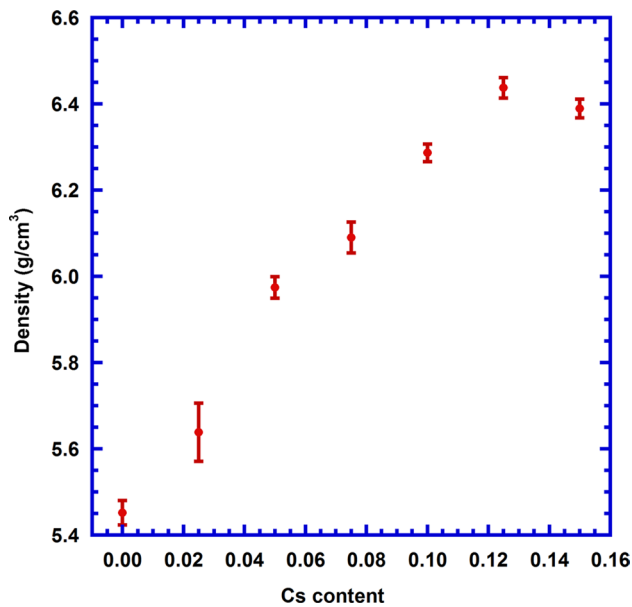


Fig. 3 Evolution of $\text{Bi}_2\text{Sr}_{2-x}\text{Cs}_x\text{Co}_2\text{O}_y$ samples density, together with its standard error, as a function of nominal Cs content

samples, slightly decreasing for higher Cs amounts. These data clearly confirm the drastic decrease of porosity when Cs is added, reaching values comparable to the reported for hot-pressed or melt-grown materials (96, and 97%, respectively) [25, 26], and only lower than the reported in partially melted materials with subsequent hot-pressing process (around 99%) [25]. Furthermore, it should be highlighted that these very high density values have been obtained through a very simple and short process, when compared to those previously mentioned in literature.

Electrical resistivity variations of all samples with temperature, as a function of Cs content, are shown in Fig. 4. As can be seen in the plot, the general sample's behaviour is significantly changed by Cs substitution; it is semi-conducting ($d\rho/dT < 0$) for the pure and 0.025 Cs samples (much less evident for these last samples), while higher Cs substitution leads to metallic ($d\rho/dT > 0$) one. Moreover, the increase of Cs substitution leads to lower electrical resistivity values than the measured in undoped ones. This evolution is in agreement with the Sr^{2+} substitution by Cs^+ , which decreases the oxidation state of the rock salt structure, promoting the Co^{3+} in the conducting layer to Co^{4+} . Consequently, the charge carrier concentration (holes), are increased, decreasing electrical resistivity. On the other hand, the increase determined in the 0.15 Cs substituted samples can be associated to the raise in the number of defects, which is responsible for their higher electrical resistivity values. Other favourable effects for this decrease in electrical resistivity are the raise in density, and the important grain growth, which decreases

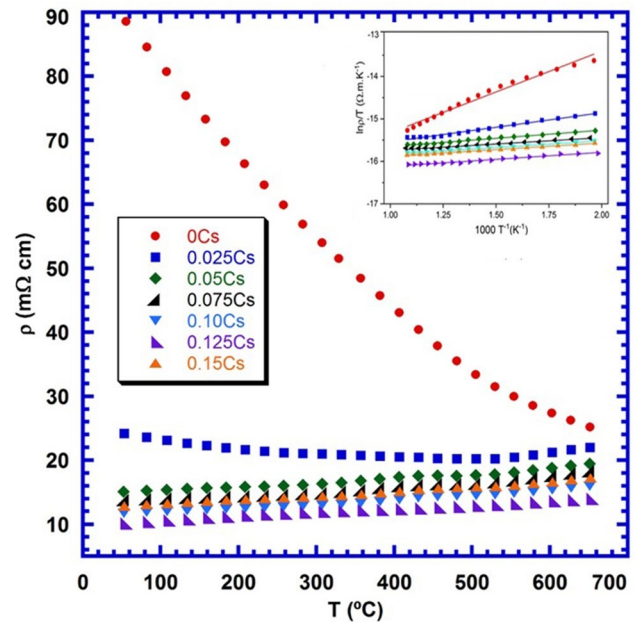


Fig. 4 Electrical resistivity evolution with temperature for $\text{Bi}_2\text{Sr}_{2-x}\text{Cs}_x\text{Co}_2\text{O}_y$ samples. The inset shows the linear fits of $\ln(\rho/T)$ versus $1000/T$ for all samples

the number of grain boundaries in the bulk material. The lowest resistivity values at 650 °C (14 mΩ cm) have been determined in 0.125 Cs substituted samples, about 40% lower than those obtained in undoped samples in this work. Moreover, they are much lower than the reported in textured materials via hot pressing (40 mΩ cm [27]), or laser processing (20 mΩ cm [13]), while they are close to those obtained in sintered materials under oxygen (15 mΩ cm [28]), or in single crystals (18 mΩ cm at room temperature [29], and 10 mΩ cm at 600 °C [16]). These results clearly agree with the drastic enhancement of grain sizes, decrease of porosity and, probably, the improvement of grains electrical connectivity, produced by Cs substitution.

The tendency observed in electrical resistivity with Cs substitution may be due to the modification of microstructure and electronic parameters. However, more information and experimental work is necessary to precisely determine and explain this evolution. Therefore, in order to better understand the mechanism of resistivity, the small polaron hopping model [30] has been used though the following relation:

$$\rho(T) = \left(\frac{T}{Anex^2} \right) \exp \left(\frac{E_a}{k_B T} \right) \tag{2}$$

where A , n , e , x , E_a , k_B , and T are the pre-exponential term related to the scattering mechanism, carrier concentration, elementary charge, intersite hopping distance,

polaron activation energy, Boltzmann constant and absolute temperature, respectively. As it is shown in the inset of Fig. 4, the linear relationship of $\ln(\rho/T)$ with respect to $1/T$ above 500 K fits well with the polaron hopping model of electrical resistivities for all samples. In order to calculate the activation energies of samples, the slopes of straight lines have been used, and the calculated values for the pure, 0.025, 0.050, 0.075, 0.10, 0.125, and 0.15 samples are 165.62, 59.21, 33.20, 25.80, 27.21, 26.60, and 25.72 meV, respectively. According to these values, the E_a values of undoped samples are much higher than the determined in Cs doped ones. Initially, the values drastically decrease up to 0.05 Cs, remaining practically constant for higher doping. The hopping of charge carriers takes place between Co^{3+} and Co^{4+} in the CoO_2 layer of BiSrCoO system. Therefore, the ratio between Co^{3+} and Co^{4+} directly influences the hopping distance, x . The decrease of this ratio suggests an increment of Co^{4+} concentration due to Cs substitution, reducing the hopping distance. This fact also leads to the decrease of hopping activation energy. This result supports the argument that the Co^{3+} is promoted to Co^{4+} in the conducting layer, as discussed above.

Figure 5 illustrates Seebeck coefficient variation with temperature, and Cs substitution. In the graph, it can be observed that all values are positive in the whole measured temperature range, which is characteristic of hole-dominating transport mechanism. At room temperature, the Seebeck coefficient is decreased in Cs substituted samples, when compared to the undoped ones. This is in agreement with Koshibae's expression [18], which indicates that the increase of Co^{4+} proportion in the

conduction band leads to a reduction of Seebeck coefficient. However, room temperature Seebeck coefficient values are only slightly modified in the Cs doped samples, which could be interpreted as a close Cs content in all doped samples, when compared to the nominal composition. This fact could also explain the fact that lower Cs content than the nominal one has been found by EDS in the samples, as observed in previous works [24]. The highest S values at 650 °C (195 $\mu\text{V}/\text{K}$) have been measured in undoped samples, around 10% higher than those measured in Cs substituted samples in this study. These values are larger than those informed in hot-pressed samples ($\sim 150 \mu\text{V}/\text{K}$) [27], or single crystals (160 $\mu\text{V}/\text{K}$) [16], and close to those determined in sintered samples obtained by soft chemistry routes (205 $\mu\text{V}/\text{K}$) [31].

Using electrical resistivity and Seebeck coefficient values previously presented, PF evolution with temperature, and Cs substitution, has been calculated and presented in Fig. 6. As it can be seen in the plot, in spite of their lower Seebeck coefficient values, Cs substituted samples display higher PF values than the undoped ones. Moreover, PF is increased with temperature in the whole measured temperature range, and with Cs content up to 0.125, slightly decreasing for higher content. The highest PF values at 650 °C ($\sim 0.20 \text{ mW}/\text{K}^2 \text{ m}$) have been obtained in 0.125 Cs substituted samples, which are around 40% higher than those determined in undoped samples in this work. Moreover, they are much larger than the presented in hot-pressed samples (0.06 $\text{mW}/\text{K}^2 \text{ m}$) [27], and similar to the obtained in ceramics prepared through soft chemistry routes (0.20 $\text{mW}/\text{K}^2 \text{ m}$) [31], at the same temperature.

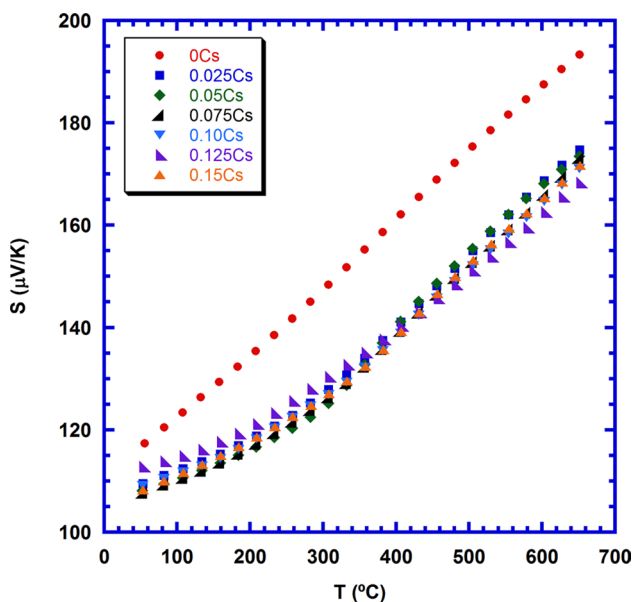


Fig. 5 Seebeck coefficient evolution with temperature for $\text{Bi}_2\text{Sr}_{2-x}\text{Cs}_x\text{Co}_2\text{O}_y$ samples

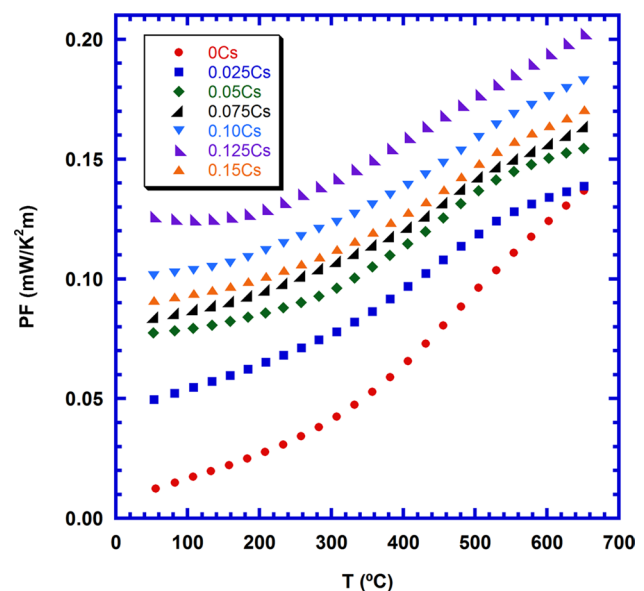


Fig. 6 Power factor evolution with temperature for $\text{Bi}_2\text{Sr}_{2-x}\text{Cs}_x\text{Co}_2\text{O}_y$ samples

However, they are still slightly lower than the best reported results in single crystals ($0.26 \text{ mW/K}^2 \text{ m}$) [16], due to the absence of grain boundaries.

Thermoelectric apparatus directly converts a temperature gradient into electricity called as the Seebeck effect, while the reverse counterpart is the thermoelectric cooling phenomenon named as Peltier effect. As it is known, the magnetic cooling is based on the Magneto Caloric Effect (MCE) and it is promisingly applicable on refrigeration systems. Hence, for the potential payoff, it is necessary to produce and optimize new thermoelectric materials, which can be suitable for operation over wide low temperature ranges. Since the thermoelectric parameters like Seebeck coefficient, power factor and others are very sensitive to the small variation of the external applied magnetic field, the magnetic characterization can be very important issue to present new candidate samples for thermoelectric-cooling applications. Therefore, the samples were investigated from the magnetic point of view. For this purpose, the temperature and field dependent magnetization, and hysteresis curves of all samples have been determined.

In Fig. 7 the magnetization of all samples with respect to temperature down to 10 K, measured in zero-field cooled mode, under 20 Oe external applied magnetic field, are presented. As it can be seen in this figure, very similar magnetic properties have been determined in all samples, i.e. magnetization of samples sharply decreases from 5 K up to 25 K, and then slowly decreases, except for 0.1 Cs ones. According to the Curie–Weiss law, in the high temperature region, the data of each sample should be fitted to a straight line by plotting inverse susceptibility ($1/\chi$) with respect to temperature, T , as given in inset of Fig. 7, for the 0.05 Cs samples. By extrapolating the high- T part of

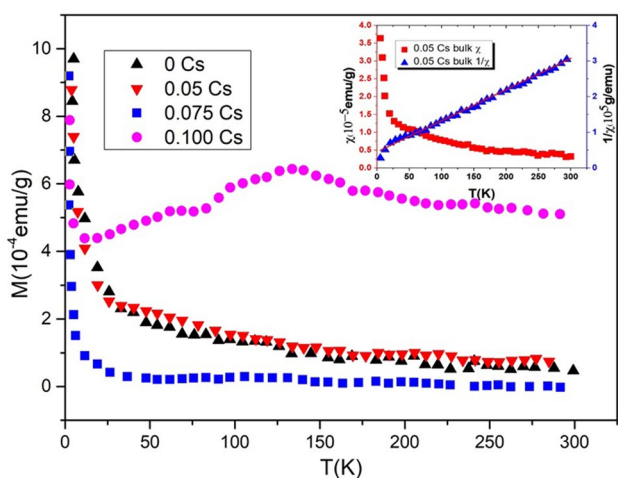


Fig. 7 DC-magnetization of pure and 0.05 Cs, 0.075 Cs, and 0.10 Cs. The inset shows the inverse DC-magnetic susceptibility curves for the 0.05 Cs doped samples measured at 20 Oe

the curves ($1/\chi \rightarrow 0$), negative paramagnetic temperatures, θ , were obtained for the pure ($\approx -60 \text{ K}$), 0.05 ($\approx -50 \text{ K}$), and 0.075 ($\approx -15 \text{ K}$), samples. Consequently, antiferromagnetic fluctuations are prevailing in these samples. However, for Cs substitution ≥ 0.10 , the $\chi(T)$ curves exhibit a shallow maximum at around 150 K. This effect may be attributed to an antiferromagnetic state promoted by this higher Cs-content.

The Curie constants of all samples have been calculated from the slope of the $1/\chi$ versus T curves, being around $\approx 3 \times 10^{-3} \text{ emu K/g}$. The effective magnetic moments, μ_{eff} for undoped, 0.05 Cs, 0.075 Cs and 0.1 Cs samples have been calculated by using the equation given in [32], as $2.40\mu_B$, $2.35\mu_B$, $1.25\mu_B$, and $3.83\mu_B$, respectively.

The $M-H$ curves, measured at 15 K for the undoped and Cs-doped samples have been plotted in Fig. 8. No hysteresis behavior can be observed in these curves, demonstrating that the paramagnetic phase is still dominant at temperatures $\geq 15 \text{ K}$. In addition, the slopes are increased when the Cs-content is higher. It is necessary to highlight that the linear field dependence of magnetization points to a normal canonical paramagnetic order in connection with the applied magnetic field.

The temperature dependence of magnetic hysteresis has been also investigated, and the results are presented in Fig. 9. Since the general behavior of undoped and Cs-doped samples is the same for Cs content up to 0.10, for the sake of clarity, only the results obtained in 0.05 Cs and 0.10 Cs samples are shown. In the figure, it can be seen that the slopes and the magnitude of magnetization is decreased when the temperature is increased for samples with Cs content ≤ 0.10 . It can be argued that when temperature decreases, the magnetic moments in random directions are affected by increasing external applied magnetic

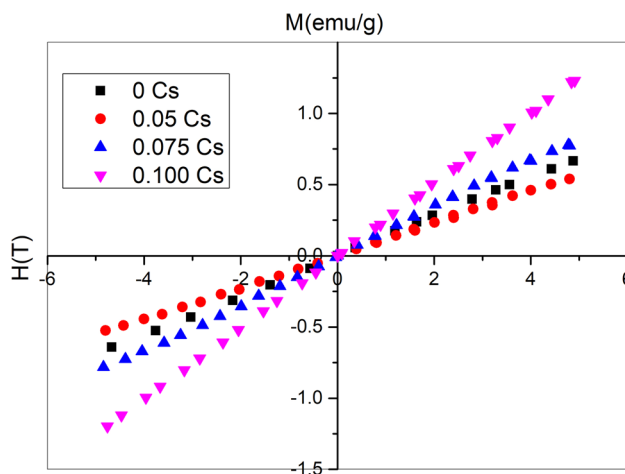


Fig. 8 Hysteresis curves for the pure and 0.05 Cs, 0.075 Cs, and 0.10 Cs samples at measured 15 K

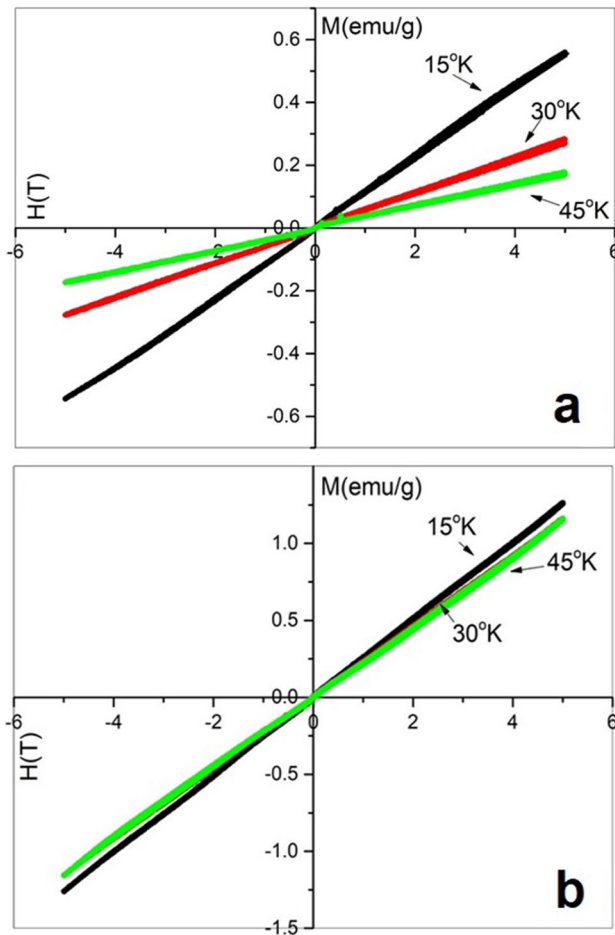


Fig. 9 Hysteresis curves for the **a** 0.05 Cs, **b** 0.10 Cs doped samples measured at 15, 30, and 45 K

field. Then, all the spins in random directions are oriented the direction of external applied magnetic field. Hence, the magnetization values start to increase with decreasing temperature values.

As a result, when considering all these results, it may be concluded that Cs-doping is very useful for improving the thermoelectric properties of $\text{Bi}_2\text{Sr}_{2-x}\text{Cs}_x\text{Co}_2\text{O}_y$ materials. An important increase in power factor, PF, obtained in this work using a simple preparation process, leads to consider these ceramic materials as very promising candidates for their integration in practical thermoelectric devices.

4 Conclusions

Bulk sintered $\text{Bi}_2\text{Sr}_{2-x}\text{Cs}_x\text{Co}_2\text{O}_y$ ($0 \leq x \leq 0.15$) thermoelectric ceramics have been successfully fabricated via the classical ceramic preparation technique. It has been found that Cs substitution has led to the formation of a liquid phase during sintering procedure, drastically enhancing

grain growth and decreasing porosity. On the other hand, this grain growth is accompanied by the formation of a Co poor region close to the grain boundaries. These microstructural modifications have been reflected in a drastic increase of relative density, reaching values of about 95% of the theoretical one. Moreover, electrical resistivity is decreased with Cs doping, due to the increase in charge carrier concentration, which has been confirmed by the decrease of Seebeck coefficient when compared to the undoped samples. Furthermore, the increase of electrical resistivity in 0.125 Cs samples is associated to the raise of defects which act as electronic scattering centers. All these characteristics led to high power factor values in Cs substituted samples, which makes them promising ceramic materials for practical applications.

On the other hand, magnetic properties do not reflect these improvements since Cs-addition is randomly influencing them.

Acknowledgements This study was carried out within the scope of Cukurova University Scientific Research Projects Unit FBA-2020-13007 and FBA-2020-12784. The authors wish to thank the Spanish MINECO-FEDER (MAT2017-82183-C3-1-R), and Gobierno de Aragón (Research Group T 54-17 R) for funding. The authors wish to acknowledge the use of Servicio General de Apoyo a la Investigación-SAI, Universidad de Zaragoza.

Compliance with ethical standards

Conflict of interest The authors declare that they have no conflict of interest.

Open Access This article is licensed under a Creative Commons Attribution 4.0 International License, which permits use, sharing, adaptation, distribution and reproduction in any medium or format, as long as you give appropriate credit to the original author(s) and the source, provide a link to the Creative Commons licence, and indicate if changes were made. The images or other third party material in this article are included in the article's Creative Commons licence, unless indicated otherwise in a credit line to the material. If material is not included in the article's Creative Commons licence and your intended use is not permitted by statutory regulation or exceeds the permitted use, you will need to obtain permission directly from the copyright holder. To view a copy of this licence, visit <http://creativecommons.org/licenses/by/4.0/>.

References

1. Altenkirch E (1909) Über den Nutzeffekt der Thermosäule. Phys Z 10(16):560–568
2. Altenkirch E (1911) Electrothermische Kalteerzeugung und reversible elektrische Heizung. Phys Z 12:920–924
3. Fu T, Yue X, Wu H, Fu C, Zhu T, Liu X, Hu L, Ying P, He J, Zhao X (2016) Enhanced thermoelectric performance of PbTe bulk materials with figure of merit $zT > 2$ by multi-functional alloying. J Materiomics 2:141–149

- Nikitin E (1958) Investigation on temperature dependencies of electrical conductivity and thermopower of silicides. *Zhurnal Tekhnicheskoy Fiziki* 28:23–25
- Terasaki I, Sasago Y, Uchinokura K (1997) Large thermoelectric power in NaCo_2O_4 single crystals. *Phys Rev B* 56:12685–12687
- LeBlanc S (2014) Thermoelectric generators: linking material properties and systems engineering for waste heat recovery applications. *Sust Mater Technol* 1–2:26–35
- Rowe DM (eds) (2006) *Thermoelectrics handbook: macro to nano*, 1st edn. CRC Press, Boca Raton
- He J, Liu Y, Funahashi R (2011) Oxide thermoelectrics: the challenges, progress, and outlook. *J Mater Res* 26:1762–1772
- Funahashi R, Matsubara I, Sodeoka S (2000) Thermoelectric properties of $\text{Bi}_2\text{Sr}_2\text{Co}_2\text{O}_x$ polycrystalline materials. *Appl Phys Lett* 76:2385–2387
- Funahashi R, Shikano M (2002) $\text{Bi}_2\text{Sr}_2\text{Co}_2\text{O}_y$ whiskers with high thermoelectric figure of merit. *Appl Phys Lett* 81:1459
- Sotelo A, Rasekh Sh, Torres MA, Bosque P, Madre MA, Diez JC (2015) Effect of synthesis methods on the $\text{Ca}_3\text{Co}_4\text{O}_9$ thermoelectric ceramic performances. *J Solid State Chem* 221:247–254
- Wu NY, Holgate TC, Nong NV, Pryds N, Linderoth S (2014) High temperature thermoelectric properties of $\text{Ca}_3\text{Co}_4\text{O}_{9+\delta}$ by auto-combustion synthesis and spark plasma sintering. *J Eur Ceram Soc* 34:925–931
- Rasekh Sh, Costa FM, Ferreira NM, Torres MA, Madre MA, Diez JC, Sotelo A (2015) Use of laser technology to produce high thermoelectric performances in $\text{Bi}_2\text{Sr}_2\text{Co}_{1.8}\text{O}_x$. *Mater Des* 75:143–148
- Wang H, Sun X, Yan X, Huo D, Li X, Li J-G, Ding X (2014) Fabrication and thermoelectric properties of highly textured $\text{Ca}_9\text{Co}_{12}\text{O}_{28}$ ceramic. *J Alloy Compd* 582:294–298
- Xu GJ, Funahashi R, Shikano M, Matsubara I, Zhou YQ (2002) Thermoelectric properties of $\text{Bi}_{2-2-x}\text{Pb}_x\text{Sr}_2\text{Co}_2\text{O}_y$ system. *J Appl Phys* 91:4344–4347
- Sun N, Dong ST, Zhang BB, Chen YB, Zhou J, Zhang ST, Gu ZB, Yao SH, Chen YF (2013) Intrinsically modified thermoelectric performance of alkaline-earth isovalently substituted $[\text{Bi}_2\text{AE}_2\text{O}_4][\text{CoO}_2]_y$ single crystals. *J Appl Phys* 114:043705
- Maignan A, Pelloquin D, Hebert S, Klein Y, Hervieu M (2006) Thermoelectric power in misfit cobaltites ceramics: optimization by chemical substitutions. *Bol Soc Esp Ceram* 45:122–125
- Koshibae W, Tsutsui K, Maekawa S (2000) Thermopower in cobalt oxides. *Phys Rev B* 62:6869–6872
- Çetin Karakaya G, Özçelik B, Nane O, Sotelo A, Rasekh Sh, Torres MA, Madre MA (2018) Improvement of $\text{Bi}_2\text{Sr}_2\text{Co}_2\text{O}_y$ thermoelectric performances by Na doping. *J Electroceram* 40:11–15
- Li Y-N, Wu P, Zhang S-P, Chen S, Yan D, Yang J-G, Wang L, Huai X-L (2018) Thermoelectric properties of lower concentration K-doped $\text{Ca}_3\text{Co}_4\text{O}_9$ ceramics. *Chin Phys B* 27:057201
- Sotelo A, Rasekh Sh, Constantinescu G, Torres MA, Madre MA, Diez JC (2013) Improvement of textured $\text{Bi}_{1.6}\text{Pb}_{0.4}\text{Sr}_2\text{Co}_{1.8}\text{O}_x$ thermoelectric performances by metallic Ag additions. *Ceram Int* 39:1597–1602
- Mercurio D, Champarnaud-Mesjard JC, Frit B, Conflant P, Boivin JC, Vogt T (1994) Thermal evolution of the crystal-structure of the rhombohedral $\text{Bi}_{0.75}\text{Sr}_{0.25}\text{O}_{1.375}$ phase—a single-crystal neutron-diffraction study. *J Solid State Chem* 112:1–8
- Hammond CR (2009) *Handbook of physics and chemistry*, 90th edn. CRC Press, Boca Raton, FL
- Sotelo A, Costa FM, Ferreira NM, Kovalevsky A, Ferro MC, Amaral VS, Amaral JS, Rasekh Sh, Torres MA, Madre MA, Diez JC (2016) Tailoring $\text{Ca}_3\text{Co}_4\text{O}_9$ microstructure and performances using a transient liquid phase sintering additive. *J Eur Ceram Soc* 36:1025–1032
- Combe E, Funahashi R, Barbier T, Azough F, Freer R (2016) Decreased thermal conductivity in $\text{Bi}_2\text{Sr}_2\text{Co}_2\text{O}_x$ bulk materials prepared by partial melting. *J Mater Res* 31:1296–1305
- Çetin G, Özçelik B, Gursul M, Torres MA, Madre MA, Sotelo A (2020) Effect of annealing and potassium substitution on the thermoelectric and magnetic properties of directionally grown $\text{Bi}_2\text{Sr}_2\text{Co}_2\text{O}_y$ ceramics. *Bol Soc Esp Ceram Vid* 59:121–128
- Shin W, Murayama N (2000) Thermoelectric properties of (Bi, Pb)–Sr–Co–O oxide. *J Mater Res* 15:382–386
- Itahara H, Xia C, Sugiyama J, Tani T (2004) Fabrication of textured thermoelectric layered cobaltites with various rock salt-type layers by using $\beta\text{-Co}(\text{OH})_2$ platelets as reactive templates. *J Mater Chem* 14:61–66
- Itoh T, Terasaki I (2000) Thermoelectric properties of $\text{Bi}_{2.3-x}\text{Pb}_x\text{Sr}_{2.6}\text{Co}_2\text{O}_y$ single crystals. *Jpn J Appl Phys* 39:6658–6660
- Bosman AJ, Daal HJV (1970) Small-polaron versus band conduction in some transition-metal oxides. *Adv Phys* 19:1
- Madre MA, Rasekh Sh, Diez JC, Sotelo A (2010) New solution method to produce high performance thermoelectric ceramics: a case study of Bi–Sr–Co–O. *Mater Lett* 64:2566–2568
- Çetin Karakaya G, Özçelik B, Torres MA, Madre MA, Sotelo A (2018) Effect of Na-doping on thermoelectric and magnetic performances of textured $\text{Bi}_2\text{Sr}_2\text{Co}_2\text{O}_y$ ceramics. *J Eur Ceram Soc* 38:515–520

Publisher's Note Springer Nature remains neutral with regard to jurisdictional claims in published maps and institutional affiliations.